

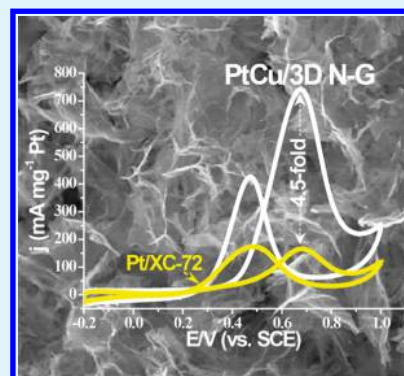
# Microwave-Assisted Synthesis of Highly Dispersed PtCu Nanoparticles on Three-Dimensional Nitrogen-Doped Graphene Networks with Remarkably Enhanced Methanol Electrooxidation

Xinglan Peng, Duhong Chen, Xiulin Yang,\*<sup>ORCID</sup> Dongsheng Wang, Mengliu Li, Chien-Chih Tseng, Rajapandiyan Panneerselvam, Xiao Wang, Wenjing Hu, Jianniao Tian, and Yanchun Zhao\*

Guangxi Key Laboratory of Low Carbon Energy Materials, College of Chemistry and Pharmacy, Guangxi Normal University, Guilin 541004, P. R. China

**ABSTRACT:** A well-dispersed PtCu alloy nanoparticles (NPs) on three-dimensional nitrogen-doped graphene (PtCu/3D N-G) electrocatalyst has been successfully synthesized by a conventional hydrothermal method combined with a high-efficiency microwave-assisted polyol process. The morphology, composition, and structures are well-characterized by scanning electron microscopy, transmission electron microscopy, Raman spectroscopy, X-ray powder diffraction, and X-ray photoelectron spectroscopy. Cyclic voltammograms illustrate that the as-prepared PtCu/3D N-G electrocatalyst possesses the larger electrochemical active surface area, lower onset potential, higher current density, and better tolerance to CO poisoning than PtCu NPs on reduced graphene oxide and XC-72 carbon black in acid solution. In addition, long-time chronoamperometry reveals that the PtCu/3D N-G catalyst exhibits excellent stability even longer than 60 min toward acid methanol electrooxidation. The remarkably enhanced performance is related to the combined effects of uniformly interconnected three-dimensional porous graphene networks, nitrogen doping, modified Pt alloy NPs, and strong binding force between Pt alloy NPs and 3D N-G structures.

**KEYWORDS:** direct methanol fuel cells, three-dimensional nitrogen-doped graphene, microwave-assisted synthesis, PtCu alloy nanoparticles, methanol electrooxidation



## INTRODUCTION

With the increasing demand for sustainable energy and severe pollution of the environment, the development of human society is facing serious challenges due to the rapid depletion of traditional energy and industrial emissions. Hence, intensive research have been conducted to explore nonpolluting and renewable energy sources.<sup>1,2</sup> The energy generated by direct methanol fuel cells (DMFCs) has introduced extensive interests because of their simple apparatus fabrication, high-efficiency energy conversion, and environmentally friendly emissions properties.<sup>3,4</sup> Most of the researchers illustrated that noble metal platinum (Pt) showed excellent electrocatalytic activity for methanol oxidation below 80 °C.<sup>5</sup> Nevertheless, the scarceness and sluggish kinetics of Pt severely suppressed its wide applications in acid DMFCs.<sup>6</sup> Thus, designing Pt-based catalysts with an efficient method is necessary to reduce the amount of usage and improve the electrocatalytic activity of Pt, such as PtRu, PtPd, PtCo, etc.<sup>7–9</sup> Recently, PtCu alloy catalysts have attracted particular attentions because the formed bimetallic structures of Pt and Cu could favor the electronic effect of downshifting the d-band center of Pt and suppress formation of Pt oxides.<sup>10</sup> Additionally, it is well-known that an optimized catalyst support could both reduce the noble catalyst consumption and enhance its electrocatalytic performance.<sup>11,12</sup> Therefore, selecting an appropriate catalyst carrier and

optimizing a suitable synthetic method are crucial for obtaining a high-performance fuel cell catalyst.

In recent years, fabricating 3D graphene materials has been a hot research topic because the inherent 2D graphene nanosheets endow them with excellent performance in various aspects.<sup>13</sup> As an efficient and controllable technique for the self-assembly of reduced graphene oxide (rGO) nanosheets into 3D porous graphene frameworks, the classical hydrothermal method has attracted immense and persistent attention.<sup>14,15</sup> Their unique hierarchical structures could not only prevent the graphene nanosheets with serious restacking but also allow multidimensional electron transport pathways and electrolytes freely diffusing inside the network.<sup>16</sup> The fabricated 3D porous graphene has demonstrated broad application potentials in supercapacitors,<sup>17</sup> lithium-ion batteries,<sup>18</sup> fuel cells,<sup>19</sup> detectors, and sensors.<sup>20,21</sup> To further tailor the electronic properties and manipulate the surface chemistry of 3D graphene, many strategies including physical or chemical methods have been applied to modify graphene materials intrinsically.<sup>22</sup> The most accepted method is introducing electron-rich nitrogen in the graphene lattice to replace its carbon atoms.<sup>23</sup> The introduced

**Received:** September 17, 2016

**Accepted:** November 18, 2016

**Published:** November 18, 2016

nitrogen could alter the crystalline and electronic structures of the carbons and enhance their surface polarity, electron-donor properties, electric conductivity, and chemical stability.<sup>24</sup> In this regard, most of the published 3D N-doped graphene showed a better performance in oxygen reduction reaction,<sup>25</sup> oxygen evolution reaction,<sup>26</sup> Li-ion batteries, etc.<sup>27</sup> However, there are still a small number of research articles related to noble metal or its alloy on 3D N-doped graphene for methanol electrooxidation in acid solution.

In this work, 3D nitrogen-doped graphene (3D N-G) networks are successfully prepared by an economical and environmentally friendly one-step hydrothermal method. Well-dispersed PtCu alloy NPs are fabricated on 3D N-G hydrogels (PtCu/3D N-G) with a high-efficiency microwave-assisted polyol process. The designed PtCu/3D N-G electrocatalyst exhibits remarkably enhanced electrocatalytic performance and high tolerance to CO poisoning toward the methanol electrooxidation compared to those PtCu NPs on rGO and XC-72 carbon black in acid solution. Moreover, the PtCu/3D N-G electrocatalyst exhibits outstanding long-term stability in 0.5 M H<sub>2</sub>SO<sub>4</sub> + 1.0 M CH<sub>3</sub>OH mixed solution.

## EXPERIMENTAL SECTION

**Preparation of Graphene Oxide (GO).** GO was synthesized via a modified Hummers method.<sup>28</sup> Initially, graphite powder (0.1 g) was mixed with 3 mL of H<sub>2</sub>SO<sub>4</sub> (98%) in an ice/water bath under slow stirring. Then, KMnO<sub>4</sub> (0.3 g) was slowly added into the obtained mixture solution and the temperature of the solution was maintained below 20 °C under continuous stirring. After that, the mixture was heated to 35 °C for 30 min, and after adding the distilled water (DI) (5 mL), the solution was kept at the same condition for 2 h. Finally, another 11 mL of DI water was slowly added, followed by 1 mL of H<sub>2</sub>O<sub>2</sub>. The color of the suspension slowly turned into bright yellow after the peroxide was added. The GO was then obtained after centrifugation and purification with DI water for several times.

**Preparation of 3D N-G Hydrogels and Aerogels.** 3D N-G hydrogels were synthesized by a conventional hydrothermal process, in which 30 mg of GO, a certain amount of CuCl<sub>2</sub>·2H<sub>2</sub>O, and 9 g of CO(NH<sub>2</sub>)<sub>2</sub> were added in one step into DI water under mild ultrasonication for ca. 30 min. The mixture solution was then poured into a cleaned Teflon-lined stainless steel autoclave with no more than 80% of its capacity, heated to 180 °C at a heating rate of 6 °C min<sup>-1</sup>, and maintained at this temperature for 12 h. A black gel-like cylinder (3D N-G hydrogels) could be found in the autoclave after it was naturally cool down to room temperature. The 3D N-G aerogels could be obtained after the 3D N-G hydrogels were dialyzed in DI water for 3 days and freeze-dried at -50 °C for 12 h.

**Synthesis of PtCu/3D N-G Electrocatalyst.** The PtCu/3D N-G electrocatalyst was prepared by a facile microwave-assisted process. In detail, 16.0 mg of 3D N-G, 1.06 mL of H<sub>2</sub>PtCl<sub>6</sub>·6H<sub>2</sub>O (19.3 mM), 7.0 mg of CuCl<sub>2</sub>·2H<sub>2</sub>O, and 20.0 mg of glutamate were added into 20 mL of ethylene glycol (EG) simultaneously. The pH value of the mixture solution was adjusted to ca. 13 by dropping 8 wt % KOH/EG solution after it was vigorously stirred for 12 h. The suspension was then sealed in a beaker, placed into a microwave oven (Galanz, 800 W), and treated by microwave irradiation for 200 s. The PtCu/3D N-G sample was received after the suspension was centrifuged and rinsed several times with copious DI water and subsequently freeze-dried in an oven for 12 h. Similar procedures were also employed for preparation of PtCu/rGO, PtCu/XC-72, and Pt/XC-72 samples.

**Characterization.** Scanning electron microscopy (SEM, Quanta FEG 200, Holland) and transmission electron microscopy (TEM, JEOL, JEM-2100F) were used to investigate the morphologies and microstructures of the designed materials. Raman spectroscopy was acquired from an inVia confocal Raman microscope (Renishaw, England). X-ray powder diffraction (XRD) data was detected by a D/Max 2500 V PC with Cu K $\alpha$  radiation from Rigaku. The chemical

valencies of the samples were examined by X-ray photoelectron spectroscopy (XPS, model: JPS-9010 TR Photoelectron Spectrometer, Japan). Inductively coupled plasma analysis (ICP) was used to determine the metal loading of the as-prepared catalyst with an instrument model for IRIS Intrepid II XSP, and the nitrogen content in the 3D graphene structures was analyzed by an elemental analyzer (PE2400II).

**Electrochemical Measurements.** A CHI 660D electrochemical workstation (CH Instrument, Inc.) was operated to measure all the electrochemical data, and the widely adopted three-electrode device was utilized in this work. The working electrode was prepared by a catalyst ink modified glassy carbon electrode (GCE,  $\phi = 3$  mm). Before dip-coating the catalyst, the GCE was initially polished with  $\alpha$ -Al<sub>2</sub>O<sub>3</sub> powder with different particle sizes, followed by sonication in C<sub>2</sub>H<sub>5</sub>OH, H<sub>2</sub>SO<sub>4</sub>, and DI-H<sub>2</sub>O for 5 min, successively. Then, a certain amount of catalyst was dissolved into ethanol/H<sub>2</sub>O (v/v = 4:1) mixture solution and then ultrasonicated for 30 min before the suspension was dropped onto the polished GCE surface. In order to avoid exfoliation of the catalyst, 5  $\mu$ L of 0.5% Nafion solution (diluted by ethanol/H<sub>2</sub>O) was then dropped onto the catalyst surface. A calomel electrode with saturated KCl solution (SCE) and a Pt sheet (1 cm  $\times$  2 cm) were selected as the reference electrode and counter electrode, respectively. All the present data were recorded in electrochemical experiments with respect to the SCE reference electrode.

Cyclic voltammetry (CV) curves with different cycles were first conducted in N<sub>2</sub>-saturated H<sub>2</sub>SO<sub>4</sub> solution with a scan rate of 50 mV s<sup>-1</sup> in the range of -0.2 to 1.0 V. The electrochemical active surface area (EAS) was evaluated from the required hydrogen adsorption and desorption charge of the repeated CV curves in N<sub>2</sub>-saturated H<sub>2</sub>SO<sub>4</sub> solution. The electrocatalytic performances of the as-prepared electrocatalysts for methanol electrooxidation were evaluated in a 0.5 M H<sub>2</sub>SO<sub>4</sub> contained 1.0 M CH<sub>3</sub>OH solution (N<sub>2</sub>-saturated) with a scan rate of 50 mV s<sup>-1</sup> from the reproducible CV curves at ca. 12–15 cycles. Chronoamperometry measurements were then performed in the N<sub>2</sub>-protected 0.5 M H<sub>2</sub>SO<sub>4</sub> + 1.0 M CH<sub>3</sub>OH solution at a fixed potential of 0.6 V for 60 min. The Pt loading of all catalysts was kept at  $\sim$ 0.071 mg cm<sup>-2</sup> on the electrode surface, and all the experiments were carried out at room temperature (25  $\pm$  1 °C).

## RESULTS AND DISCUSSION

**Synthesis and Characterization of PtCu/3D N-G.** Photos of GO before and after hydrothermal treatment are shown in Figure 1a,b. As shown in Figure 1a, the precursor of GO with a typical yellow solution was transformed into a black gel-like cylinder (see Figure 1b) after hydrothermal treatment at 180 °C for 12 h. According to the apparent changes in color

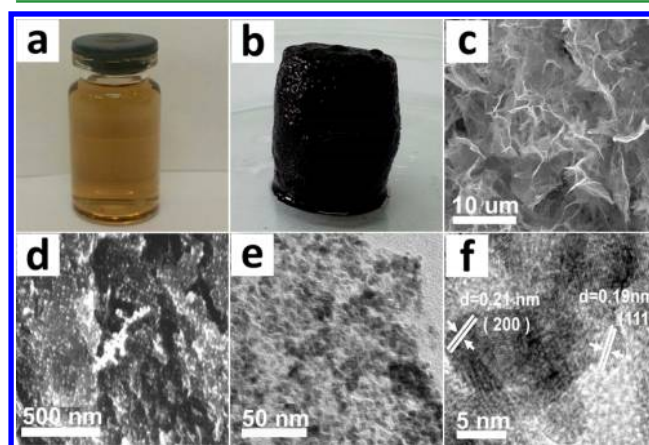
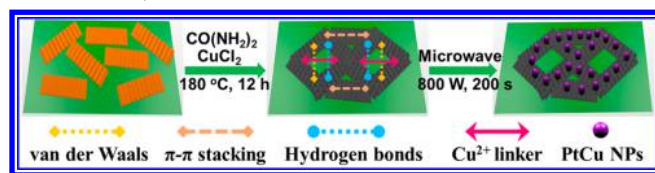


**Figure 1.** Photographs of (a) GO solution and (b) 3D N-G hydrogels. SEM images of (c) 3D N-G aerogels and (d) PtCu/3D N-G. TEM (e) and high-resolution TEM (f) images of PtCu/3D N-G.

and structures, the reaction mechanism can be explained as follows: initially, the partially reduced GO nanosheets are coalesced or overlapped, and then the robust cross-links of 3D graphene networks are formed with the help of a  $\text{Cu}^{2+}$  linker,  $\pi$ - $\pi$  stacking, van der Waals' forces, and abundant hydrogen bonding from water during the hydrothermal treatment (Scheme 1).<sup>29</sup> As shown in Figure 1c, the freeze-dried 3D N-

### Scheme 1. Schematic of the Formation of PtCu/3D N-G Electro catalyst



G aerogels exhibit well-defined and interconnected 3D network microstructures, which could effectively prevent restacking of graphene sheets, endue most of the graphene nanosheets adequately contacted with the electrolyte, and provide open channels for free transfer of electrolyte.<sup>30</sup> The SEM (see Figure 1d) and TEM (see Figure 1e) images indicate that the well-dispersed PtCu NPs almost cover all of the 3D N-G sheets with a uniform size distribution for  $5 \pm 0.5$  nm. The high-resolution TEM image of PtCu NPs (see Figure 1f) displays clear lattice fringes with fringe spacings of ca. 0.21 and 0.19 nm related to the (111) and (200) interplanar distances of face-centered cubic (fcc) PtCu alloy, respectively, which reveals the formation of PtCu alloy.<sup>31</sup> Inductively coupled plasma (ICP) is usually used to measure metal loading on the catalyst support. Generally, the targeted catalysts are calcined in air to remove the combustible substrate, dissolved in aqua regia, and then transferred into a volumetric flask for testing. In this experiment, the results show that the Pt is 20.8% and Cu is 12.9% for PtCu/3D N-G, which is consistent with the calculated theoretical results. Additionally, the elemental analyzer is applied to analyze the amount of nitrogen content in the 3D graphene structures, and the results indicate that the nitrogen contents are 10.99% and 11.05% for 3D N-G and PtCu/3D N-G, respectively.

### Raman Spectra and XRD Crystal Structure Analysis.

Raman spectra of the different synthesized samples including GO, rGO, and 3D N-G with and without supported PtCu NPs are detailedly investigated in Figure 2A. There are two characteristic peaks belonging to graphene, located at 1350 and 1594  $\text{cm}^{-1}$ , referring to the D-band and G-band, respectively.<sup>32</sup> It is well-known that the D-band induced by the disordered structures of graphene corresponds to  $\text{sp}^3$  carbon atom vibrations and the G-band derived from the domains of graphite is associated with vibrations of  $\text{sp}^2$  carbon atoms.<sup>33</sup> Commonly, the ratio of peak intensity of the D-band versus the G-band ( $I_D/I_G$ ) is selected as a ruler to measure the degree of graphitization of carbon materials.<sup>11</sup> From Figure 2A, the  $I_D/I_G$  ratio of rGO (1.49) is apparently higher than that of GO (1.15), indicating that the exfoliated GO is reduced to a lower average size of  $\text{sp}^2$  domains for rGO.<sup>34</sup> However, the 3D N-G exhibits a lower  $I_D/I_G$  ratio (1.01) and wider D-band than GO and rGO simultaneously. The lower ratio illustrates that the generated 3D network structures could better maintain larger  $\text{sp}^2$  domains after GO reduction, and the wider D-band could be ascribed to the structural distortion caused by N-doping and edge defects that originated from the 3D network

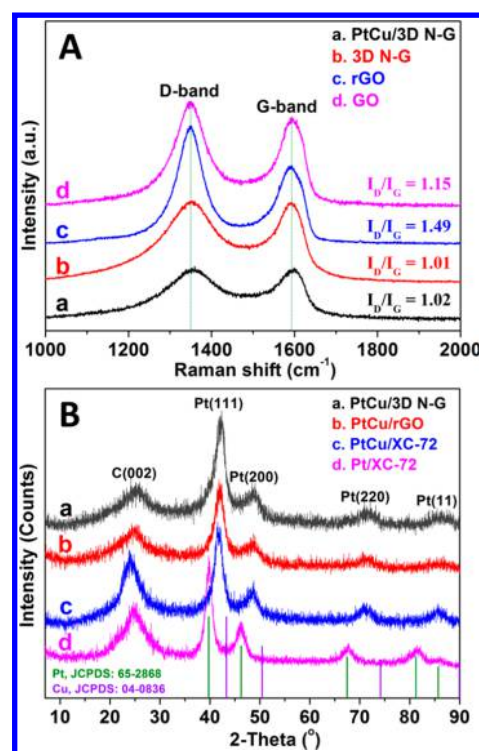


**Figure 2.** (A) Raman spectra of (a) PtCu/3D N-G, (b) 3D N-G, (c) rGO, and (d) GO. (B) X-ray diffraction (XRD) patterns of the as-prepared (a) PtCu/3D N-G, (b) PtCu/rGO, (c) PtCu/XC-72, and (d) Pt/XC-72. The standard patterns of pure Pt and Cu are inserted for comparison.

structures.<sup>35</sup> After PtCu alloy particles deposition, a slight blue shift could be observed on PtCu/3D N-G, which should be derived from an interaction between the metal particles and the support.<sup>36</sup>

Crystal structures of metal NPs and carbon substrate were investigated by XRD. Figure 2B shows the XRD patterns of the synthesized PtCu/3D N-G together with PtCu/rGO, PtCu/XC-72, and Pt/XC-72 for comparison. It can be easily noted that all the samples have similar XRD patterns, including carbon (002) and face-centered cubic (fcc) crystal structure Pt with (111), (200), (220), and (311) peaks.<sup>37</sup> It should be emphasized that the carbon (002) plane of 3D N-G has a broader peak at ca.  $25.2^\circ$  than XC-72, indicating that a short-range order is presented in the typical features of stacked layers of N-doped graphene.<sup>38</sup> Furthermore, there is no additional peak at ca.  $10.0^\circ$  which belongs to GO, confirming the recovered graphitic crystal structures during the hydrothermal process.<sup>39</sup> The most interesting features are observed that all peak positions of the PtCu specimens are shifted to higher  $2\theta$  degrees than the Pt/XC-72, demonstrating that the replaced Pt atoms by smaller Cu atoms could cause a lattice shrinkage.<sup>40</sup> The reduced lattice parameters could reduce the Pt interatomic distance, and thus enable the tuning of the catalytic activity.<sup>41</sup> What's more, the typical diffraction peaks of Cu metal or its oxide are not shown in all the XRD patterns, which suggests that some of the PtCu alloys are formed or a partially amorphous phase of Cu-oxides coexisted.<sup>42</sup> As discussed above, the PtCu alloy structure is indeed formed when heated by microwave irradiation in a short time. The average particle size of the formed PtCu alloy NPs is estimated by the Scherrer equation<sup>43</sup>

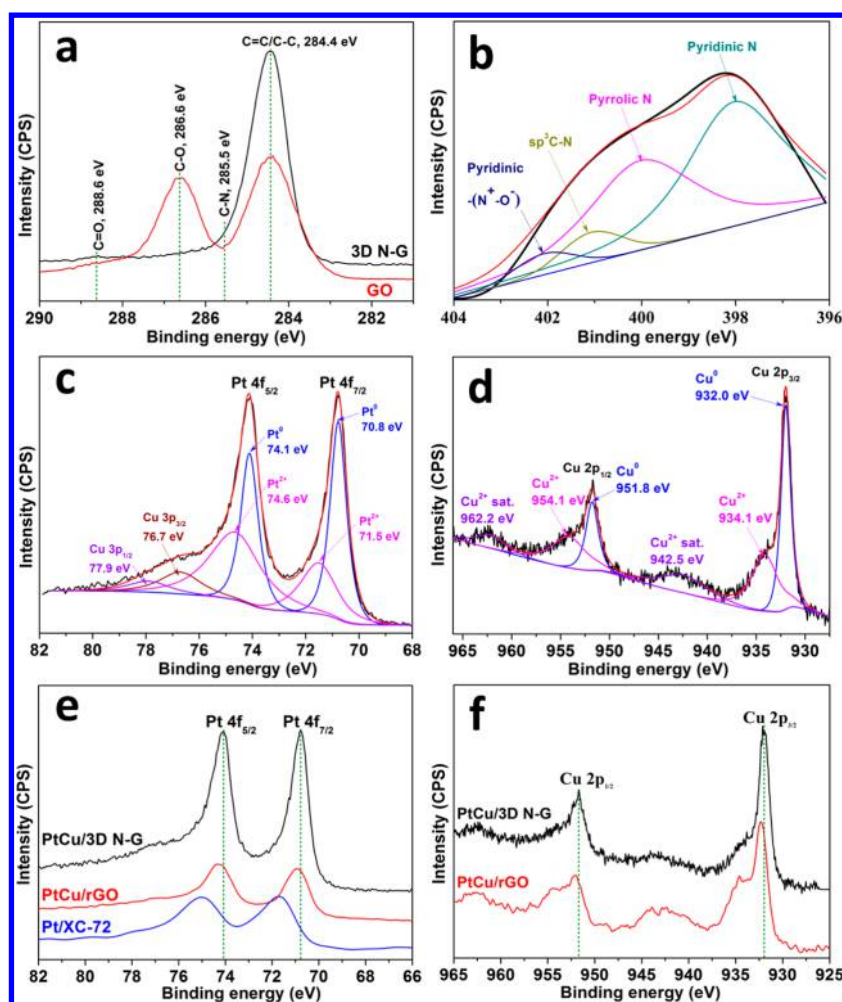


**Figure 3.** (a) High-resolution XPS spectra of C 1s orbital of GO and 3D N-G. (b) High-resolution XPS spectra of (b) N 1s, (c) Pt 4f, and (d) Cu 2p orbitals of PtCu/3D N-G. Comparison of the subspectra of (e) Pt 4f and (f) Cu 2p orbitals from PtCu/3D N-G, PtCu/rGO, and Pt/XC-72, respectively.

$$D = K\lambda/\beta \cos \theta$$

where  $D$  is the calculated average diameter of the related particles in nm,  $\lambda$  is the used wavelength of X-ray (0.154056 nm),  $K$  is the Scherrer constant (0.89),  $\theta$  is the Bragg diffraction angle, and  $\beta$  is the half height width of the peak with radians as a unit. The selected diffraction peak of Pt(111) reveals that the mean sizes of different catalysts are as follows: PtCu/3D N-G (4.8 nm), PtCu/rGO (5.7 nm), PtCu/XC-72 (6.2 nm), and Pt/XC-72 (8.5 nm). The calculated particle size of PtCu/3D N-G is consistent with the observed TEM result, and the smaller particle size on the 3D N-G support is similar to the metal NPs on the N-doped pyrolytic graphite.<sup>44</sup>

**Chemical State Analysis by XPS Technique.** XPS measurements were employed to identify the states of the elements in bulk material, and the typical results are shown in Figure 3. As shown in Figure 3a, a sharp peak at about 284.4 eV is assigned to the mixed C=C/C-C bonds with sp<sup>2</sup>/sp<sup>3</sup> hybrid carbon in the C 1s spectrum of GO, which is consistent with the synthesized 3D N-G result. The other peaks at higher binding energy correspond to C-O bond configurations with different models including C-O (hydroxyls/epoxy, ~286.6 eV) and C=O (ketone/carbonyl, ~288.6 eV), respectively.<sup>45</sup> However, a significant decrement in the intensity of the carbon-oxygen peak (C-O at 286.6 eV) indicates that GO has

been efficiently reduced and the graphitic carbon network has partially been restored in 3D N-G structures.<sup>14</sup> The additional binding energy at 285.5 eV could be ascribed to the N-sp<sup>2</sup> C in the N-doped 3D graphene structures.<sup>46</sup>

As shown in Figure 3b, the chemical states of nitrogen in the hybrid catalyst are analyzed. The pyridinic-N (~398.1 eV) and pyrrolic-N (~400.0 eV) could effectively contribute electron density from their lone pair electrons to the  $\pi$ -conjugated system in the 2D graphene layers.<sup>38</sup> The binding energy at 401.1 eV is associated with nitrogen directly substituted sp<sup>2</sup> hybridized carbon,<sup>23</sup> and the peak position at 402.1 eV is corresponding to the nitrogen oxides of pyridinic-nitrogen.<sup>47</sup> The incorporated nitrogen inside graphite structures is the quaternary-N species, and the occupied edge plane sites are the pyridinic-N species carrying extra lone pair electrons. From the high-resolution XPS spectrum of N 1s for PtCu/3D N-G, the dominant pyridinic-N species could induce much stronger interaction between the deposited metal NPs and the substrate, thereby inhibiting the agglomeration of the metal NPs, and efficiently improve the performance of the electrocatalyst.

The high-resolution XPS spectrum of Pt 4f was analyzed by curve deconvolution fitting as shown in Figure 3c. The contained metal Pt<sup>0</sup> exhibits two stronger peaks with the binding energies at 70.8 and 74.1 eV corresponding to Pt 4f<sub>7/2</sub> and Pt 4f<sub>5/2</sub>, respectively. Meanwhile, the double peaks at 71.5

eV (Pt 4f<sub>7/2</sub>) and 74.6 eV (Pt 4f<sub>5/2</sub>) are contributed to the Pt<sup>2+</sup> species in the form of PtO or Pt(OH)<sub>2</sub>.<sup>48</sup> Especially, it should be noted that two broad peaks at higher binding energies of 76.7 and 77.9 eV should be ascribed to Cu 3p<sub>3/2</sub> and Cu 3p<sub>1/2</sub>, respectively. Additionally, the chemical state of Cu 2p was also probed and is shown in Figure 3d. The distinct twin peaks at 932.0 eV (Cu 2p<sub>3/2</sub>) and 951.8 eV (Cu 2p<sub>1/2</sub>) are observed, relating to Cu<sup>0</sup> in the synthesized PtCu/3D N-G.<sup>49</sup> The subsequent binding energies at 934.1 eV (Cu 2p<sub>3/2</sub>) and 954.1 eV (Cu 2p<sub>1/2</sub>) combined with two relative “satellite peaks” are the characteristic features of Cu<sup>2+</sup> species.<sup>42,50</sup> Interestingly, the high-resolution XPS spectrum of Pt 4f for PtCu/3D N-G located at 70.8 eV (Pt 4f<sub>7/2</sub>) and 74.1 eV (Pt 4f<sub>5/2</sub>) shows about 0.2 and 0.9 eV negative shift compared to PtCu/rGO and Pt/XC-72, respectively (see Figure 3e). The similar negative shift is also observed on Cu 2p<sub>3/2</sub> and Cu 2p<sub>1/2</sub> of PtCu/3D N-G compared to PtCu/rGO (see Figure 3f). As previously reported in the literature, the downshift of the d-band center position of Pt could promote the desorption of CO and oxygen from the targeted catalysts surface, and thus favor high electrochemical activity for methanol electrooxidation.<sup>51</sup>

**Electrochemical Performance Analysis.** The surface electrochemical properties of the PtCu/3D N-G electrocatalyst were initially studied by the CV method with different potential cycles in the range of -0.2 to 1.0 V in N<sub>2</sub>-saturated 0.5 M H<sub>2</sub>SO<sub>4</sub> solution. As shown in Figure 4A, there is a clear peak step in the forward scan at about 0.0 V in the first and second cycles, and then it disappeared at the seventh cycle. It is believed that the changes of the peak step originated from the electrochemical dissolving of the undetectable or amorphous Cu crystallites or their oxide. The peak potential at about 0.45 V in the forward scan could be ascribed to electrochemical

oxidation of the uncovered Cu atoms on the surface of the PtCu alloy catalyst.<sup>52</sup> At the potential higher than 0.6 V, the surface Pt atoms from the PtCu alloy catalyst will be further oxidized to Pt oxides/hydroxides.<sup>53</sup> In the reverse scan, the generated Pt oxides/hydroxides are reduced at about 0.5 V, and the oxidized Cu atoms in the PtCu alloy are redeposited at about 0.3 V.<sup>41</sup> The overlapped seventh cycle and eighth cycle indicates that the Pt atoms on the surface of PtCu/3D N-G are rearranged and enriched with the dissolution of the Cu atoms to an undetectable level.<sup>41</sup> The hypothetical Pt shell structure will be gradually formed with the conducted dealloying process on the PtCu alloy surface. The resultant nearly pure Pt on the catalyst surface is desirable for great improvement of the electrocatalytic performance due to the geometric effect by the expanding or compressing arrangement of surface Pt atoms.<sup>54</sup> Strasser et al. have found that the d-band center and the lattice strain of Pt from the dealloyed Pt-alloy catalyst could significantly improve the electrocatalytic activity in fuel cells.<sup>55</sup> As shown in Figure 4B, the repeatedly dealloyed CV curves of three PtCu alloys and pure Pt catalysts show the characteristic peaks for hydrogen adsorption/desorption, double layer range, and the redox peaks for the Cu and Pt contained surface. The electrochemical active surface area (EAS) values of each catalyst were estimated by the following equation

$$\text{EAS} = Q_{\text{H}} / (0.21 \times m_{\text{Pt}})$$

where  $m_{\text{Pt}}$  is the Pt loading (mg cm<sup>-2</sup>) on the working electrode,  $Q_{\text{H}}$  (mC cm<sup>-2</sup>) is obtained by integrating the corrected hydrogen adsorption/desorption region and then divided by the used scan rate for different electrocatalysts, and 0.21 (mC cm<sup>-2</sup>) is the required charge to oxidize a monolayer of hydrogen on a smooth Pt surface. As displayed in Figure 4B, the calculated specific EAS values are 47.8 m<sup>2</sup> g<sup>-1</sup> for PtCu/3D N-G, 39.5 m<sup>2</sup> g<sup>-1</sup> for PtCu/rGO, 30.2 m<sup>2</sup> g<sup>-1</sup> for PtCu/XC-72, and 52.6 m<sup>2</sup> g<sup>-1</sup> for Pt/XC-72 electrocatalysts, respectively. The lower EAS values for PtCu alloy electrocatalysts compared to Pt catalyst are most likely owing to some formed aggregation in the electrochemical process and/or surface coated by organic species.<sup>56</sup>

The electrocatalytic activities of the PtCu/3D N-G, PtCu/rGO, PtCu/XC-72, and Pt/XC-72 catalysts toward methanol electrooxidation were investigated in N<sub>2</sub>-saturated acid solution in the range of -0.2 to 1.0 V. As shown in Figure 5A, the onset potential ( $E_{\text{onset}}$ ) of the PtCu/3D N-G catalyst negatively shifts about 100 mV than Pt NPs on XC-72 carbon black, indicating that the PtCu/3D N-G catalyst is more kinetically effective.<sup>57</sup> Interestingly, the PtCu/3D N-G catalyst also shows the lowest forward peak potential ( $E_{\text{f}}$ ) than others, implicating that the methanol dehydrogenation and formation of OH<sub>ads</sub> are facilitated by the reaction kinetics.<sup>58</sup> The forward peak current density ( $j_{\text{f}}$ ) is assigned to the electrocatalytic oxidation of CH<sub>3</sub>OH molecules on the catalysts modified electrode surface, while the backward peak current density ( $j_{\text{b}}$ ) is ascribed to electrooxidation of the accumulated carbonaceous species, which are incompletely oxidized in the forward scan, such as HCOO<sup>-</sup>, HCO<sup>-</sup>, and CO species.<sup>51</sup> All the CV curves show that the PtCu alloy-based electrocatalysts reveal much higher forward peak current densities than Pt NPs on XC-72 carbon black. It should be noted that the designed PtCu/3D N-G catalyst displays the highest current density than others and ca. 4.5-fold higher than the Pt/XC-72 catalyst especially. These surprising results suggest that the designed PtCu/3D N-G

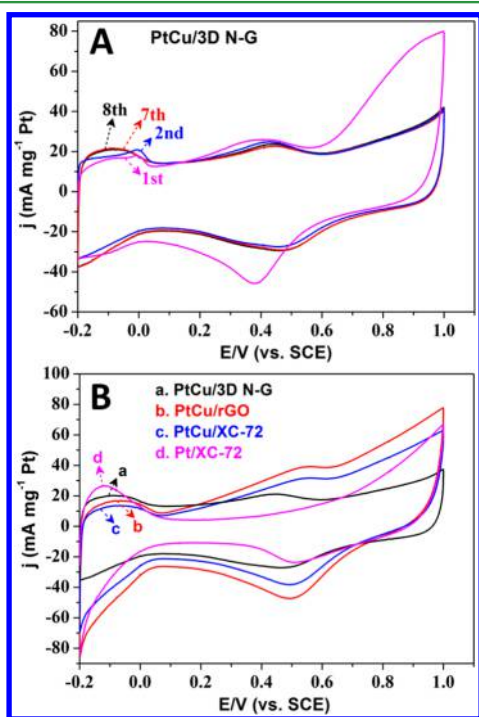


**Figure 4.** (A) CV curves of PtCu/3D N-G electrocatalyst at different potential cycles and (B) CV curves of (a) PtCu/3D N-G, (b) PtCu/rGO, (c) PtCu/XC-72, and (d) Pt/XC-72 in 0.5 M H<sub>2</sub>SO<sub>4</sub> solution with a scan rate of 50 mV s<sup>-1</sup>. All the current densities in the curves have been normalized by the loading mass of Pt.

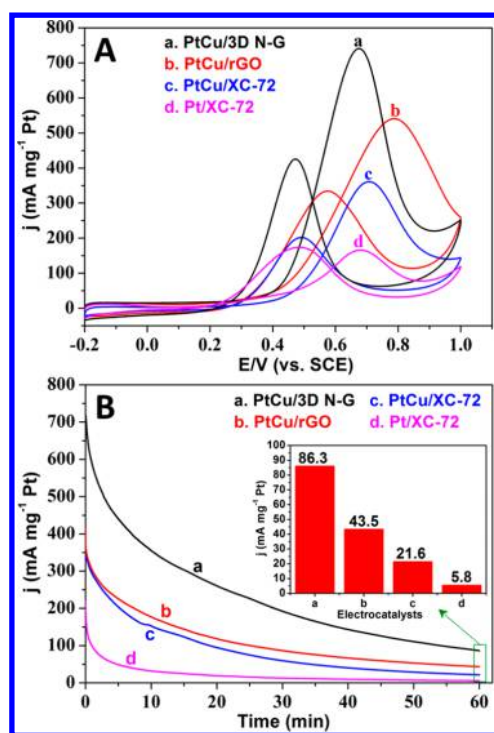


**Figure 5.** (A) CV curves with a scan rate of  $50 \text{ mV s}^{-1}$  and (B) chronoamperometric curves at  $0.6 \text{ V}$  of (a) PtCu/3D N-G, (b) PtCu/rGO, (c) PtCu/XC-72, and (d) Pt/XC-72 electrocatalysts in  $0.5 \text{ M H}_2\text{SO}_4 + 1.0 \text{ M CH}_3\text{OH}$  solution. Inset image of (B) is the last values chronoamperometric curves of these four electrocatalysts.

hybrid catalyst could efficiently adsorb and oxidize  $\text{CH}_3\text{OH}$  molecules in the forward scan.<sup>59</sup> Additionally, the antipoisoning ability of a designed electrocatalyst is described by the ratio of  $j_f/j_b$ , which represents the catalyst tolerance to intermediate carbonaceous species that were generated in the forward scan.<sup>60</sup> The summarized results (see Table 1) illustrate that the

**Table 1.** Characteristic Values for As-Prepared Various Electrocatalysts

electrocatalysts	$E_{\text{onset}}$ (V)	$E_f$ (V)	$j_f$ ( $\text{mA mg}^{-1} \text{ Pt}$ )	$j_f/j_b$
PtCu/3D N-G	0.38	0.67	741.2	1.75
PtCu/rGO	0.40	0.79	542.7	1.61
PtCu/XC-72	0.42	0.71	362.7	1.77
Pt/XC-72	0.48	0.68	166.5	0.95

designed PtCu/3D N-G catalyst exhibits a higher  $j_f/j_b$  ratio than the Pt/XC-72 electrocatalyst, which implies that the PtCu alloy catalysts could better oxidize the  $\text{CH}_3\text{OH}$  molecules to  $\text{CO}_2$  than only Pt NPs in the forward potential scan.<sup>61</sup>

The long-term durability of the designed electrocatalyst is another crucial factor affecting its practical applications. Thus, the electrocatalytic activity for methanol electrooxidation was further examined by chronoamperometric measurements in  $\text{N}_2$ -saturated  $0.5 \text{ M H}_2\text{SO}_4 + 1.0 \text{ M CH}_3\text{OH}$  solution at  $0.6 \text{ V}$  for 60 min. As shown in Figure 5B, the current densities of all the electrocatalysts decay rapidly in the initial period and then reached almost steady states. The initial higher current densities of the electrocatalysts are due to the initial high concentration of  $\text{CH}_3\text{OH}$  molecules on the electrocatalysts' surface; after that, the quick decay of the current densities is because of the decreased concentration gradient and poisoning by the

accumulated intermediate species on the surface of the electrocatalysts.<sup>62</sup> It should be particularly pointed out that the current density of the PtCu/3D N-G electrocatalyst is significantly higher than that of all the compared electrocatalysts during the whole time, and the final current density of the PtCu/3D N-G ( $86.3 \text{ mA mg}^{-1} \text{ Pt}$ ) is 1.98-, 3.99-, and 14.89-fold higher than that of the PtCu/rGO, PtCu/XC-72, and Pt/XC-72, respectively. In a word, the PtCu/3D N-G electrocatalyst exhibits a higher electrocatalytic activity and better stability than other compared catalysts for methanol electrooxidation.

The excellent electrocatalytic activity and long-term durability for methanol electrooxidation on the PtCu/3D N-G electrocatalyst could be summarized as follows: (a) 3D interconnected graphene networks with open porous channels are more favorable for the electron and  $\text{CH}_3\text{OH}$  molecules transport, resulting in a further improvement of the catalyst utilization.<sup>19</sup> (b) The incorporated nitrogen atoms in the 3D graphene networks could alter the electron-donating characteristics of the substrate, which, in turn, strengthens the binding force between the metal NPs and the substrate. The enhanced binding energy could lead to a better dispersion and induce a smaller metal particle size distribution on the N-doped graphene structures. (c) A compressive strain is produced in the PtCu/3D N-G catalyst when some Pt is replaced by small Cu atoms according to Vegard's law based on XRD results. The generated higher lattice strain could apparently lower the bonding energy with the intermediate oxygenated adsorbates, favor the removal of the incompletely oxidized carbonaceous species, and thus strengthen the resistivity to the poisoning of intermediates carbonaceous species.<sup>63</sup> (d) The Pt d-band center of the PtCu alloy is moderately shifted down compared to the pure Pt catalyst with the XPS analysis, which suggests that the designed PtCu alloy catalyst could reduce the possibility of carbonaceous species adsorption. In the meantime, it will not decrease too much methanol chemisorption.<sup>64</sup> (e) The adsorption properties of Pt atoms on the catalyst's surface have been changed by alloying with Cu. This results in an intermetallic charge transfer and the interatomic distances change for the surface atoms, which could further increase the intrinsic activities of the PtCu/3D N-G electrocatalyst.<sup>65</sup>

## CONCLUSION

In summary, we demonstrated a facile one-step approach for the fabrication of 3D N-G hydrogels through a self-assembly hydrothermal process. The PtCu alloy NPs were successfully synthesized and deposited onto 3D N-G hydrogels by a high-efficiency microwave-assisted process. The as-prepared PtCu/3D N-G electrocatalyst exhibits an enhanced electrocatalytic activity, a good durability, and a high tolerance to carbonaceous poisoning for the  $\text{CH}_3\text{OH}$  electrooxidation in acid solution compared to PtCu/rGO, PtCu/XC-72, and Pt/XC-72 catalysts. This enhanced electrocatalytic performance toward the  $\text{CH}_3\text{OH}$  electrooxidation could be credited to the combined effects of uniform interconnected 3D porous graphene networks, nitrogen doping, strong interaction between metal NPs and 3D N-G, and the modified Pt alloy. The facile synthesis and high performance of the PtCu/3D N-G electrocatalyst suggest the possibility of replacing contemporary electrocatalysts in fuel cells for practical applications.

## AUTHOR INFORMATION

## Corresponding Authors

\*E-mail: xiulin.yang@kaust.edu.sa (X.Y.).

\*E-mail: yanchunzhaoh@aliyun.com (Y.Z.).

## ORCID

Xiulin Yang: 0000-0003-2642-4963

## Notes

The authors declare no competing financial interest.

## ACKNOWLEDGMENTS

This work has been supported by the National Natural Science Foundation of China (21363003, 21165004, 21163002), the Natural Science Foundation of Guangxi Province (2014GXNSFGA118008, 2014GXNSFFA118003), the BAGUI scholar program (2014A001), and the Project of Talents Highland of Guangxi Province.

## REFERENCES

- (1) Palacin, M. R. Recent advances in rechargeable battery materials: a chemist's perspective. *Chem. Soc. Rev.* **2009**, *38*, 2565–75.
- (2) Chen, Z.; Higgins, D.; Yu, A.; Zhang, L.; Zhang, J. A review on non-precious metal electrocatalysts for PEM fuel cells. *Energy Environ. Sci.* **2011**, *4*, 3167–3192.
- (3) Hunt, S. T.; Milina, M.; Alba-Rubio, A. C.; Hendon, C. H.; Dumesic, J. A.; Román-Leshkov, Y. Self-assembly of noble metal monolayers on transition metal carbide nanoparticle catalysts. *Science* **2016**, *352*, 974–978.
- (4) Cui, X.; Guo, W.; Zhou, M.; Yang, Y.; Li, Y.; Xiao, P.; Zhang, Y.; Zhang, X. Promoting Effect of Co in  $Ni_mCo_n$  ( $m + n = 4$ ) Bimetallic Electrocatalysts for Methanol Oxidation Reaction. *ACS Appl. Mater. Interfaces* **2015**, *7*, 493–503.
- (5) Hogarth, M. P.; Hards, G. A. Direct methanol fuel cells. Technological advances and further requirements. *Platinum Met. Rev.* **1996**, *40*, 150–159.
- (6) Franceschini, E. A.; Bruno, M. M.; Williams, F. J.; Viva, F. A.; Corti, H. R. High-Activity Mesoporous Pt/Ru Catalysts for Methanol Oxidation. *ACS Appl. Mater. Interfaces* **2013**, *5*, 10437–10444.
- (7) Zhao, Y.; Yang, X.; Tian, J.; Wang, F.; Zhan, L. A facile and novel approach toward synthetic polypyrrole oligomers functionalization of multi-walled carbon nanotubes as PtRu catalyst support for methanol electro-oxidation. *J. Power Sources* **2010**, *195*, 4634–4640.
- (8) Yang, X.; Liu, X.; Meng, X.; Wang, X.; Li, G.; Shu, C.; Jiang, L.; Wang, C. Self-assembly of highly dispersed Pt and PtRu nanoparticles on perylene diimide derivatives functionalized carbon nanotubes as enhanced catalysts for methanol electro-oxidation. *J. Power Sources* **2013**, *240*, 536–543.
- (9) Qiu, H.; Zou, F. Retraction of Nanoporous PtCo Surface Alloy Architecture with Enhanced Properties for Methanol Electrooxidation. *ACS Appl. Mater. Interfaces* **2013**, *5*, 6775–6775.
- (10) Jia, Y.; Jiang, Y.; Zhang, J.; Zhang, L.; Chen, Q.; Xie, Z.; Zheng, L. Unique Excavated Rhombic Dodecahedral  $PtCu_3$  Alloy Nanocrystals Constructed with Ultrathin Nanosheets of High-Energy {110} Facets. *J. Am. Chem. Soc.* **2014**, *136*, 3748–3751.
- (11) Zhao, Y.; Yang, X.; Tian, J. Electrocatalytic oxidation of methanol at 2-aminophenoxazin-3-one-functionalized multiwalled carbon nanotubes supported PtRu nanoparticles. *Electrochim. Acta* **2009**, *54*, 7114–7120.
- (12) Yang, X.; Wang, X.; Zhang, G.; Zheng, J.; Wang, T.; Liu, X.; Shu, C.; Jiang, L.; Wang, C. Enhanced electrocatalytic performance for methanol oxidation of Pt nanoparticles on  $Mn_3O_4$ -modified multi-walled carbon nanotubes. *Int. J. Hydrogen Energy* **2012**, *37*, 11167–11175.
- (13) He, Y.; Chen, W.; Li, X.; Zhang, Z.; Fu, J.; Zhao, C.; Xie, E. Freestanding Three-Dimensional Graphene/MnO<sub>2</sub> Composite Networks As Ultralight and Flexible Supercapacitor Electrodes. *ACS Nano* **2013**, *7*, 174–182.
- (14) Cong, H.-P.; Ren, X.-C.; Wang, P.; Yu, S.-H. Macroscopic Multifunctional Graphene-Based Hydrogels and Aerogels by a Metal Ion Induced Self-Assembly Process. *ACS Nano* **2012**, *6*, 2693–2703.
- (15) Zhou, X.; Tang, S.; Yin, Y.; Sun, S.; Qiao, J. Hierarchical porous N-doped graphene foams with superior oxygen reduction reactivity for polymer electrolyte membrane fuel cells. *Appl. Energy* **2016**, *175*, 459–467.
- (16) Wu, Z.-S.; Sun, Y.; Tan, Y.-Z.; Yang, S.; Feng, X.; Müllen, K. Three-Dimensional Graphene-Based Macro- and Mesoporous Frameworks for High-Performance Electrochemical Capacitive Energy Storage. *J. Am. Chem. Soc.* **2012**, *134*, 19532–19535.
- (17) Xu, Y.; Lin, Z.; Huang, X.; Liu, Y.; Huang, Y.; Duan, X. Flexible Solid-State Supercapacitors Based on Three-Dimensional Graphene Hydrogel Films. *ACS Nano* **2013**, *7*, 4042–4049.
- (18) Luo, J.; Liu, J.; Zeng, Z.; Ng, C. F.; Ma, L.; Zhang, H.; Lin, J.; Shen, Z.; Fan, H. J. Three-Dimensional Graphene Foam Supported  $Fe_3O_4$  Lithium Battery Anodes with Long Cycle Life and High Rate Capability. *Nano Lett.* **2013**, *13*, 6136–6143.
- (19) Maiyalagan, T.; Dong, X.; Chen, P.; Wang, X. Electrodeposited Pt on three-dimensional interconnected graphene as a free-standing electrode for fuel cell application. *J. Mater. Chem.* **2012**, *22*, 5286–5290.
- (20) Cao, X.; Zeng, Z.; Shi, W.; Yep, P.; Yan, Q.; Zhang, H. Three-Dimensional Graphene Network Composites for Detection of Hydrogen Peroxide. *Small* **2013**, *9*, 1703–1707.
- (21) Yuan, M.; Liu, A.; Zhao, M.; Dong, W.; Zhao, T.; Wang, J.; Tang, W. Bimetallic PdCu nanoparticle decorated three-dimensional graphene hydrogel for non-enzymatic amperometric glucose sensor. *Sens. Actuators, B* **2014**, *190*, 707–714.
- (22) Tan, Y.; Xu, C.; Chen, G.; Fang, X.; Zheng, N.; Xie, Q. Facile Synthesis of Manganese-Oxide-Containing Mesoporous Nitrogen-Doped Carbon for Efficient Oxygen Reduction. *Adv. Funct. Mater.* **2012**, *22*, 4584–4591.
- (23) Usachov, D.; Vilkov, O.; Grüneis, A.; Haberer, D.; Fedorov, A.; Adamchuk, V. K.; Preobrajenski, A. B.; Dudin, P.; Barinov, A.; Oehzelt, M.; Laubschat, C.; Vyalikh, D. V. Nitrogen-Doped Graphene: Efficient Growth, Structure, and Electronic Properties. *Nano Lett.* **2011**, *11*, 5401–5407.
- (24) Xia, Y.; Mokaya, R. Synthesis of Ordered Mesoporous Carbon and Nitrogen-Doped Carbon Materials with Graphitic Pore Walls via a Simple Chemical Vapor Deposition Method. *Adv. Mater.* **2004**, *16*, 1553–1558.
- (25) Wu, Z.-S.; Yang, S.; Sun, Y.; Parvez, K.; Feng, X.; Müllen, K. 3D Nitrogen-Doped Graphene Aerogel-Supported  $Fe_3O_4$  Nanoparticles as Efficient Electrocatalysts for the Oxygen Reduction Reaction. *J. Am. Chem. Soc.* **2012**, *134*, 9082–9085.
- (26) Chen, S.; Duan, J.; Jaroniec, M.; Qiao, S. Z. Three-Dimensional N-Doped Graphene Hydrogel/NiCo Double Hydroxide Electrocatalysts for Highly Efficient Oxygen Evolution. *Angew. Chem., Int. Ed.* **2013**, *52*, 13567–13570.
- (27) Xu, J.; Wang, M.; Wickramaratne, N. P.; Jaroniec, M.; Dou, S.; Dai, L. High-Performance Sodium Ion Batteries Based on a 3D Anode from Nitrogen-Doped Graphene Foams. *Adv. Mater.* **2015**, *27*, 2042–2048.
- (28) Cote, L. J.; Kim, F.; Huang, J. Langmuir–Blodgett Assembly of Graphite Oxide Single Layers. *J. Am. Chem. Soc.* **2009**, *131*, 1043–1049.
- (29) Jiang, X.; Ma, Y.; Li, J.; Fan, Q.; Huang, W. Self-Assembly of Reduced Graphene Oxide into Three-Dimensional Architecture by Divalent Ion Linkage. *J. Phys. Chem. C* **2010**, *114*, 22462–22465.
- (30) Zhang, L.; Shi, G. Preparation of Highly Conductive Graphene Hydrogels for Fabricating Supercapacitors with High Rate Capability. *J. Phys. Chem. C* **2011**, *115*, 17206–17212.
- (31) Xu, D.; Liu, Z.; Yang, H.; Liu, Q.; Zhang, J.; Fang, J.; Zou, S.; Sun, K. Solution-Based Evolution and Enhanced Methanol Oxidation Activity of Monodisperse Platinum-Copper Nanocubes. *Angew. Chem., Int. Ed.* **2009**, *48*, 4217–4221.
- (32) Zhao, Y.; Yang, X.; Zhan, L.; Ou, S.; Tian, J. High electrocatalytic activity of PtRu nanoparticles supported on starch-

functionalized multi-walled carbon nanotubes for ethanol oxidation. *J. Mater. Chem.* **2011**, *21*, 4257–4263.

(33) Yang, X.; Zheng, J.; Zhen, M.; Meng, X.; Jiang, F.; Wang, T.; Shu, C.; Jiang, L.; Wang, C. A linear molecule functionalized multi-walled carbon nanotubes with well dispersed PtRu nanoparticles for ethanol electro-oxidation. *Appl. Catal., B* **2012**, *121–122*, 57–64.

(34) Stankovich, S.; Dikin, D. A.; Piner, R. D.; Kohlhaas, K. A.; Kleinhammes, A.; Jia, Y.; Wu, Y.; Nguyen, S. T.; Ruoff, R. S. Synthesis of graphene-based nanosheets via chemical reduction of exfoliated graphite oxide. *Carbon* **2007**, *45*, 1558–1565.

(35) Zheng, Y.; Jiao, Y.; Ge, L.; Jaroniec, M.; Qiao, S. Z. Two-Step Boron and Nitrogen Doping in Graphene for Enhanced Synergistic Catalysis. *Angew. Chem., Int. Ed.* **2013**, *52*, 3110–3116.

(36) Liu, M.; Lu, Y.; Chen, W. PdAg Nanorings Supported on Graphene Nanosheets: Highly Methanol-Tolerant Cathode Electrocatalyst for Alkaline Fuel Cells. *Adv. Funct. Mater.* **2013**, *23*, 1289–1296.

(37) Gumeci, C.; Cearnaigh, D. U.; Casadonte, D. J.; Korzeniewski, C. Synthesis of PtCu<sub>3</sub> bimetallic nanoparticles as oxygen reduction catalysts via a sonochemical method. *J. Mater. Chem. A* **2013**, *1*, 2322–2330.

(38) Vinayan, B. P.; Nagar, R.; Rajalakshmi, N.; Ramaprabhu, S. Novel Platinum–Cobalt Alloy Nanoparticles Dispersed on Nitrogen-Doped Graphene as a Cathode Electrocatalyst for PEMFC Applications. *Adv. Funct. Mater.* **2012**, *22*, 3519–3526.

(39) Long, D.; Li, W.; Ling, L.; Miyawaki, J.; Mochida, I.; Yoon, S.-H. Preparation of Nitrogen-Doped Graphene Sheets by a Combined Chemical and Hydrothermal Reduction of Graphene Oxide. *Langmuir* **2010**, *26*, 16096–16102.

(40) Peng, X.; Zhao, Y.; Chen, D.; Fan, Y.; Wang, X.; Wang, W.; Tian, J. One-pot synthesis of reduced graphene oxide supported PtCu<sub>y</sub> catalysts with enhanced electro-catalytic activity for the methanol oxidation reaction. *Electrochim. Acta* **2014**, *136*, 292–300.

(41) Mani, P.; Srivastava, R.; Strasser, P. Dealloyed Pt–Cu Core–Shell Nanoparticle Electrocatalysts for Use in PEM Fuel Cell Cathodes. *J. Phys. Chem. C* **2008**, *112*, 2770–2778.

(42) Mintsouli, I.; Georgieva, J.; Armanyanov, S.; Valova, E.; Avdeev, G.; Hubin, A.; Steenhaut, O.; Dille, J.; Tsiplakides, D.; Balomenou, S.; Sotiropoulos, S. Pt–Cu electrocatalysts for methanol oxidation prepared by partial galvanic replacement of Cu/carbon powder precursors. *Appl. Catal., B* **2013**, *136–137*, 160–167.

(43) Chen, D.; Zhao, Y.; Fan, Y.; Peng, X.; Wang, X.; Tian, J. Synthesis of Ni@PbPt supported on graphene by galvanic displacement reaction for improving ethanol electro-oxidation. *J. Mater. Chem. A* **2013**, *1*, 13227–13232.

(44) Zhou, Y.; Pasquarelli, R.; Holme, T.; Berry, J.; Ginley, D.; O’Hayre, R. Improving PEM fuel cell catalyst activity and durability using nitrogen-doped carbon supports: observations from model Pt/HOPG systems. *J. Mater. Chem.* **2009**, *19*, 7830–7838.

(45) Sheng, Z.-H.; Shao, L.; Chen, J.-J.; Bao, W.-J.; Wang, F.-B.; Xia, X.-H. Catalyst-Free Synthesis of Nitrogen-Doped Graphene via Thermal Annealing Graphite Oxide with Melamine and Its Excellent Electrocatalysis. *ACS Nano* **2011**, *5*, 4350–4358.

(46) Zhang, C.; Fu, L.; Liu, N.; Liu, M.; Wang, Y.; Liu, Z. Synthesis of Nitrogen-Doped Graphene Using Embedded Carbon and Nitrogen Sources. *Adv. Mater.* **2011**, *23*, 1020–1024.

(47) Jiang, H.; Yao, Y.; Zhu, Y.; Liu, Y.; Su, Y.; Yang, X.; Li, C. Iron Carbide Nanoparticles Encapsulated in Mesoporous Fe–N-Doped Graphene-Like Carbon Hybrids as Efficient Bifunctional Oxygen Electrocatalysts. *ACS Appl. Mater. Interfaces* **2015**, *7*, 21511–21520.

(48) Hao, Y.; Yang, Y.; Hong, L.; Yuan, J.; Niu, L.; Gui, Y. Facile Preparation of Ultralong Dendritic PtIrTe Nanotubes and Their High Electrocatalytic Activity on Methanol Oxidation. *ACS Appl. Mater. Interfaces* **2014**, *6*, 21986–21994.

(49) Kuang, Y.; Cai, Z.; Zhang, Y.; He, D.; Yan, X.; Bi, Y.; Li, Y.; Li, Z.; Sun, X. Ultrathin Dendritic Pt<sub>3</sub>Cu Triangular Pyramid Caps with Enhanced Electrocatalytic Activity. *ACS Appl. Mater. Interfaces* **2014**, *6*, 17748–17752.

(50) Min, S.; Yang, X.; Lu, A.-Y.; Tseng, C.-C.; Hedhili, M. N.; Li, L.-J.; Huang, K.-W. Low overpotential and high current CO<sub>2</sub> reduction with surface reconstructed Cu foam electrodes. *Nano Energy* **2016**, *27*, 121–129.

(51) Du, S.; Lu, Y.; Steinberger-Wilckens, R. PtPd nanowire arrays supported on reduced graphene oxide as advanced electrocatalysts for methanol oxidation. *Carbon* **2014**, *79*, 346–353.

(52) Mani, P.; Srivastava, R.; Strasser, P. Dealloyed binary PtM<sub>3</sub> (M = Cu, Co, Ni) and ternary PtNi<sub>3</sub>M (M = Cu, Co, Fe, Cr) electrocatalysts for the oxygen reduction reaction: Performance in polymer electrolyte membrane fuel cells. *J. Power Sources* **2011**, *196*, 666–673.

(53) Zhao, H.; Yu, C.; You, H.; Yang, S.; Guo, Y.; Ding, B.; Song, X. A green chemical approach for preparation of Pt<sub>x</sub>Cu<sub>y</sub> nanoparticles with a concave surface in molten salt for methanol and formic acid oxidation reactions. *J. Mater. Chem.* **2012**, *22*, 4780–4789.

(54) Mavrikakis, M.; Hammer, B.; Nørskov, J. K. Effect of Strain on the Reactivity of Metal Surfaces. *Phys. Rev. Lett.* **1998**, *81*, 2819–2822.

(55) Strasser, P.; Koh, S.; Anniyev, T.; Greeley, J.; More, K.; Yu, C.; Liu, Z.; Kaya, S.; Nordlund, D.; Ogasawara, H.; Toney, M. F.; Nilsson, A. Lattice-strain control of the activity in dealloyed core-shell fuel cell catalysts. *Nat. Chem.* **2010**, *2*, 454–460.

(56) Xia, B. Y.; Wu, H. B.; Wang, X.; Lou, X. W. One-Pot Synthesis of Cubic PtCu<sub>3</sub> Nanocages with Enhanced Electrocatalytic Activity for the Methanol Oxidation Reaction. *J. Am. Chem. Soc.* **2012**, *134*, 13934–13937.

(57) Liu, X.; Xu, G.; Chen, Y.; Lu, T.; Tang, Y.; Xing, W. A Strategy for Fabricating Porous PdNi@Pt Core-shell Nanostructures and Their Enhanced Activity and Durability for the Methanol Electrooxidation. *Sci. Rep.* **2015**, *5*, 7619.

(58) Xu, C.; Wang, L.; Mu, X.; Ding, Y. Nanoporous PtRu Alloys for Electrocatalysis. *Langmuir* **2010**, *26*, 7437–7443.

(59) Huang, X.; Chen, Y.; Zhu, E.; Xu, Y.; Duan, X.; Huang, Y. Monodisperse Cu@PtCu nanocrystals and their conversion into hollow-PtCu nanostructures for methanol oxidation. *J. Mater. Chem. A* **2013**, *1*, 14449–14454.

(60) Xiao, M.; Li, S.; Zhao, X.; Zhu, J.; Yin, M.; Liu, C.; Xing, W. Enhanced Catalytic Performance of Composition-Tunable PtCu Nanowire Networks for Methanol Electrooxidation. *ChemCatChem* **2014**, *6*, 2825–2831.

(61) Hsin, Y. L.; Hwang, K. C.; Yeh, C.-T. Poly(vinylpyrrolidone)-Modified Graphite Carbon Nanofibers as Promising Supports for PtRu Catalysts in Direct Methanol Fuel Cells. *J. Am. Chem. Soc.* **2007**, *129*, 9999–10010.

(62) Li, H.-H.; Zhao, S.; Gong, M.; Cui, C.-H.; He, D.; Liang, H.-W.; Wu, L.; Yu, S.-H. Ultrathin PtPdTe Nanowires as Superior Catalysts for Methanol Electrooxidation. *Angew. Chem., Int. Ed.* **2013**, *52*, 7472–7476.

(63) Cui, C.-H.; Li, H.-H.; Yu, S.-H. Large scale restructuring of porous Pt–Ni nanoparticle tubes for methanol oxidation: A highly reactive, stable, and restorable fuel cell catalyst. *Chem. Sci.* **2011**, *2*, 1611–1614.

(64) Papadimitriou, S.; Armanyanov, S.; Valova, E.; Hubin, A.; Steenhaut, O.; Pavlidou, E.; Kokkinidis, G.; Sotiropoulos, S. Methanol Oxidation at Pt–Cu, Pt–Ni, and Pt–Co Electrode Coatings Prepared by a Galvanic Replacement Process. *J. Phys. Chem. C* **2010**, *114*, 5217–5223.

(65) Hodnik, N.; Bele, M.; Rečnik, A.; Logar, N. Z.; Gaberšček, M.; Hočevar, S. Enhanced Oxygen Reduction and Methanol Oxidation Reaction Activities of Partially Ordered PtCu Nanoparticles. *Energy Procedia* **2012**, *29*, 208–215.